2011 IEEE International Conference on Robotics and Automation
Shanghai International Conference Center
May 9-13, 2011, Shanghai, China

A Magnetic Thin Film Microrobot with Two Operating Modes

Wuming Jing, Xi Chen, Sean Lyttle, Zhenbo Fu, Yong Shi, David J. Cappelleri

***Abstract*— Magnetic principles have proved successful for untethered submillimeter microrobotics, although challenges still exist in areas of propulsion and control. This paper presents the design, analysis, and performance results for a bimorph thin film magnetic microrobot utilizing the magnetostrictive principle as a secondary oscillating operation mode. The microrobot is no larger than 580 μm in its planar dimension and its total thickness is less than 5 μm. As a robot with magnetic material, it can be operated in a pushing/pulling mode in orthogonal directions for movement in a plane, while it's powered with an external magnetic field as low as 1 mT. For the secondary oscillating operation mode utilizing the magnetostrictive principle, in-plane strain is induced , resulting in bending and blocking forces on the robot. These forces are theoretically calculated to prove enough drive force can be generated in this mode. The design is further abstracted and translated into a piezoelectric cantilever FEM model to confirm the theorectical results. Microrobot fabrication and test-bed development based on this analysis is shown, which enabled us to participate in the final competition in the 2010 NIST Mobile Microrobot Challenge, with good performance in the dash and freestyle events. Finally, we discuss the testing results in various dry and fluid environments along with recommendations for future investigation and improvements. Keywords: microrobot, magnetostrictive, bimorph**

I. INTRODUCTION

In the last decade, untethered submillimeter microrobotics has emerged with new operational modes and high operational speeds facilitated by their small size and mass. As one of the next waves in intelligent systems, microrobotics with these features are likely to have a major impact on advanced manufacturing, the health care industry and continued miniaturization of consumer products [1], and especially on biotechnology and medical applications.

Representive actuation mechanisms applied to microrobotics include electrostatic [2], [3], thermal [4], [5], [6], pieozoelectric [7] and electromagnetic [8], [9] actuation. Based on an electrostatic scratch drive actuator (SDA), Donald et al. [3] developed a microrobot working within an underlying electrical grid. Sul et al. [4] used a laser in providing power to thermal actuators of a locomotive microdevice. The laser power was also applied by Pac et al. [6] for initial microrobot design and experiments, while Erdem et al. [5] embedded chip sets with thermal microactuators using the current's heat to drive the microactuators. The electrostatically driven microrobots can be well controlled but they need electrical feeds or rely on a structured substrate which will limit their potential applications. The thermally actuated

W. Jing, S. Lyttle, Z. Fu, and D. Cappelleri are with the Multi-Scale Robotics and Automation Lab; X. Chen and Y. Shi are with the Active Nanomaterials & Devices Laboratory; Department of Mechanical Engineering, Stevens Institute of Technology, 1 Castle Point on Hudson, Hoboken, NJ USA 07030 [wjing, xchen1, slyttle, zfu, Yong.Shi, David.Cappelleri] @stevens.edu

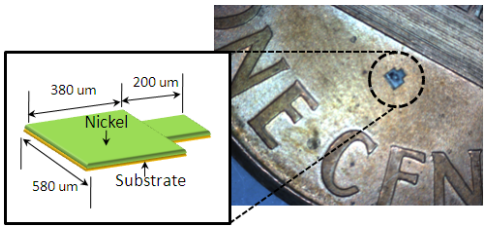

Fig. 1. μMAB microrobot

microrobots also need specific devices for precise control, like a heating resistor or an open area exposed to the designed laser source. Besides electrostatic and thermal principles, electromagnetic systems using external magnetic fields provide attractive merits for untethered microrobots [8], [9]. The group from ETH Zurich has successfully developed the the wireless resonant magnetic microactuator (WRMMA) *Magmite* family of microrobots [8]. In this design, time-variant magnetic fields are used to induce oscillatory motion and impact between the hammer and the body drives the robot forward. The microrobots from Carnegie Mellon University [10], utilizing neodymium-iron-boron (NdFeB) magnetic bodies, are controlled with low frequency magnetic fields. Both of the teams performed well in previous mobile microrobot competitions [11] organized by the National Institute of Standards and Technology (NIST).

In the real environment of manufacturing and medical applications, complex surface conditions can exist other than pure fluidic environments. Our design is intended to adapt to these and other various surroundings. Thus, our effort is focused on exploring the interface between the operating substrate and the robot where surface effects significantly affect robots behavior. This paper's microrobot design (Fig.1) is driven by a magnetic field which provides power for robot locomotion and signals for wireless remote control. In this paper, we will first present the design of the robot, followed by the theoretical and FEM validation. A description of the microrobot fabrication process follows. Next, we describe the test-bed setup and the control strategy. Finally, the performance results for the two operating modes within both a dry and fluidic environment are discussed, along with description of the problems encountered, and recommendations for future investigation provided.

II. MICROROBOT DESIGN

A magnetic part responds to a considerable magnetic field. The ETH Zurich and Carnegie Mellon University's microrobotic systems have proved that both soft and hard magnetic bodies at the micron scale can be driven by an exterior magnetic field of strengths smaller than 5 mT and work best in fluidic environments. Therefore, as the first

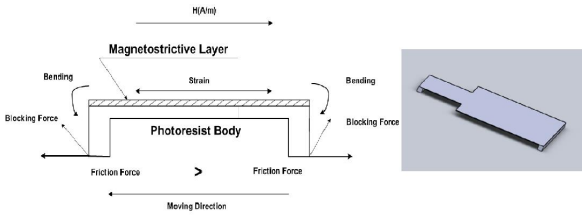

Fig. 2. (a) μMAB microrobot actuation principle; (b) μMAB schematic

working mode, our magnetic microrobot can be expected to be pulled/pushed by such an external gradient field. Further, the novelty of this paper's microrobot design is to investigate a separate oscillating operating mode, which is a walking-like moving gait based on a magnetostrictive mechanism. This mode takes advantages of the surface adhesion and friction forces and is designed for use in dry environments. The mechanism's detailed design and theoretical validation follows.

A. Actuation and Moving Principle

Inspired by Jinsoeok's [12] cell robot design, we apply magnetic fields to provide power and use the magnetostrictive principle to generate motion. In Jinsoeok's cell robot design, cardiomyocytes were cultured on an asymmetric PDMS structure with three front and rear legs. The pulsation of the cardiomyocytes would cause the legs to exhibit vertical bending displacement as a result of the contractile force. The bending causes friction and the robot motion results from the friction difference between the front legs and the rear legs.

In our design, we apply a magnetostrictive material layer to a substrate layer to generate this contractile force and bending. If the blocking forces of the front leg's bending and rear leg's are different, further, if the following friction difference is larger than the resistance caused by the surface and gravity, motion can be expected. The design and this actuation mechanism are shown in the Fig.2.

We call our robot a **micro**-scale **M**agnetic **A**symmetric thin film **B**imorph (μMAB) microrobot. Magnetostrictive bending, made from a magnetic film bonded to a nonmagnetic substrate, occurs when the film is magnetized by an applied field [13]. A magnetostrictive stress is produced in the film. Bending occurs if one end of the two layer structures is clamped. Further, if the deflected end is in contact with some ground or face, a blocking force is produced which is able to provide mechanical work through the friction force it causes. Legs with different geometry and contact lines/areas are able to lead to different blocking forces and then friction forces. Making use of the friction difference along the contact face between the robot and the supporting substrate can push or pull the robot mass.

If the robot is on the substrate and the external magnetic field is static and constant, the robot legs will remain bent; if the magnetic field is a pulsing signal on and off, the legs will perform bending and straightening, which means a walking/crawling motion will result. Further, when the surrounding magnetic field is a high frequency pulsing signal, for example, with the natural frequency of the robot, the robot would be expected to perform very fast walking and/or running motions. The direction control can be readily realized by changing the direction of magnetic field to align the magnetic body.

B. Modeling and Validation Analysis

Determining whether the microrobot has enough power/force to conquer the resistance to move is a critical step that must be validated before manufacturing the μMAB microrobot. We need to calculate how much driving force we can expect based on the commonly available surroundings, such as off-the-shelf electronic components.

To calculate the friction force caused by the blocking force, we need to evaluate the deflection of the magnetostrictive bimorph layers. Except the work in [13], few theories and software tools are able to simulate and predict planar magnetostrictive bimorph's behavior. What we do here is translate the magnetostrictive problem to a piezoelectric one, because the later situation has more available research and analysis software tools such as ANSYS (ANSYS, Inc., *www.ansys.com*) and Coventor (Coventor, Inc., *www.coventor.com*).

Like piezoelectric and its converse effect, piezomagnetic and magnetostrictive effect are opposite phenomena. Neglecting all non-linearities, hysteresis and also the effects of temperature, the piezomagnetic equations are [14]:

$$\varepsilon = \frac{\sigma}{E_y^H} + d_{33}^{\sigma} H \tag{1}$$

$$B = d_{33}^{H^*} \sigma + \mu^{\sigma} H \tag{2}$$

where ε is strain, E_y^H is Young's modulus at constant magnetic field H, B is magnetic induction, μ^{σ} is permeability at constant stress, d_{33}^{σ} is its the axial strain coefficient, d_{33}^{σ}= dε/dH, and $d_{33}^{H^*}$ is its inverse coefficient while $d_{33}^{H^*}$=dB/dσ. Now, we can look at the equations describing piezoelectric phenomena. The so-called coupled equations for piezoelectric of the strain-charge form are [15], [16]:

$$S = [s^E]T + [d^t]E \tag{3}$$

$$D = [d]T + [\epsilon^T]E \tag{4}$$

where S is strain, *s* is compliance stiffness and *T* is stress. D is the electric charge density displacement (electric displacement), ϵ is permittivity and E is zero or constant electric field strength. d is the matrix for direct piezoelectric effect and d^t is the matrix for the converse piezoelectric effect. The superscript E indicates a zero or constant electric field; the superscript T indicates a zero, or constant, stress field; and the superscript t stands for transposition of a matrix.

Comparing both of the equation sets notice that if we treat the effects as a one-dimensional property, the mathematic principles of piezoelectric and piezomagnetic are basically the same. Magnetic field corresponds to the electric field and the other relevant physical quantities correspond, respectively. These analogies are summarized in Table I. Therefore, for a simple structure, the magnetostrictive phenomenon can be calculated and simulated by the inverse piezoelectric phenomenon and method. For the robot structure shown in

TABLE I

ANALOGIES IN PIEZOMAGNETIC AND PIEZOELECTRIC DOMAINS

	Magnetostrictive-piezomagnetic	Converse-piezoelectric
Concept	magnetic field	electric field
Symbol&Unit	H(A/m)	E(V/m)
Concept	magnetic induction	electric displacement
Symbol&Unit	B(N/Am)	D(C/m^2)
Concept	piezomagnetic-strain coefficient	piezoelectric-strain coefficient
Symbol&Unit	d(Vs/N=m/A)	d(C/N=m/V)

Fig.2, we calculate the bending displacement and blocking force through the same dimension, using a silicon substrate cantilever deposited with piezoelectric layer, whose property parameters are modified appropriately. An analytical model for a PZT biomorph cantilever deflection is described in [17] as:

$$\delta = \frac{3L^2}{2t} \frac{2AB(1+B)^2}{A^2B^4 + 2A(2B + 3B^2 + 2B^3) + 1} dV \qquad (5)$$

where δ is the displacement of the beam structure, *L* is the beam length, *t* is the beam thickness (silicon+PZT), *A* is the Young's modulus ratio of silicon and PZT, *B* is the thickness ratio of silicon and PZT, *d* is the piezoelectric coefficient, and *V* is the electric field in V/m.

As long as we have these theoretical models in the piezoelectric domain, the next step is to evaluate the parameter values in the magnetostrictive domain reasonably. The geometric dimensions are the same values and the values of substrate material properties are also the same in both domains, like Young's modulus. For the magnetostrictive material, we select terfenol-D. Its physical property and magnetostrictive coefficient are evaluated according to the data sheet [18] and relevant literature [19], where the Young's modulus of terfenol-D is 30 GPa. The magnetostrictive coefficient d_{33} is 1.5E-8 Vs/N (or m/A), which corresponds to the piezoelectric-strain coefficient. The only undetermined value left is V, which corresponds to the surrounding magnetic/electric field potential difference. Based on the Ampere's circuital law [20], we see that the magnetic field with as strong as an intensity of H = 2000 A/m is able to be expected. Based on these values and (5), we get a theoretical deflection of about 5.61 μm and 1.61 μm for the front and rear legs, respectively. These results were also validated through ANSYS, using the piezo units 226 element type, whose results are 5.81 μm and 1.68 μm. Therefore, the theoretical model is able to predict the real deflection well. Moreover, to calculate the blocking force, we can apply the model in [17] using (6):

$$F = \frac{3wt^2}{8L} \frac{2AB}{(AB+1)(1+B)} Y dV \qquad (6)$$

where *F* is the maximum blocking force, and *w* the width of the beam. The maximum theoretical blocking force was calculated based on the coefficient *d* and material's Young's modulus. The calculation of the difference in blocking forces(drive force) from the asymmetric design is approximately 5 μN. We can compare this driving force with resistive force. For a conservative estimation, we let the friction coefficient = 1 and calculate the drag force to be on the order of nN's. The gravity force is calculated to be approximately 9 nN. Thus, we are able to predict that the drive force is much larger than required (μN vs nN).

In addition to the robot deflection and drive force, the lowest natural frequency and the first mode of the robot are also predicted through FEM modeling. This provides a reference for the primary excitation (control) signal for the microrobot. Fixing the front and rear feet to simulate contact with the ground surface, the simulation result shows that the first natural frequency is at about 6 kHz.

III. MICROROBOT FABRICATION

This μMAB design was fabricated with custom MEMS technics such as photolithography and Physical Vapor Deposition(PVD). The first step is the deposition of about 500 nm thick OmniCoat (MicroChem, Inc., *www.microchem.com*) layer on a bare silicon wafer as a sacrificial layer, followed by coating with one layer of negative photoresist(SU8-100, MicroChem, Inc.). In the second step, the leg structures are patterned but without development. Next, another thin layer of negative photoresist of type SU8-2 (MicroChem, Inc.) is applied. This layer of SU8-2 is only 2 μm thick, which is the thickness we set in the design and simulation for the body of the μMAB. In the following step, the SU8-2 layer is exposed to define the asymmetric body outline. The exposing time of this step is critical, especially over-exposure, because a thicker body would make the robot much harder (stiffer) to bend. After photoresist development, the shape of the robot body's outline is defined and prepared for the magnetic metal layer deposition. Before the deposition, chromium was thermal evaporated in advance in order to increase magnetic layer's adhesion. As these are our initial fabrication trials, nickel not Terfenol-D was chosen as our magnetostrictive layer due to its ease of fabrication, cost and availability. Moreover, our simulation showed the design is able to generate much more power than required, so applying nickel rather than Terfenol-D will be sufficient to actuate the robot, although it's magnetostrictive strain coefficient is lower. Ideally, the pure nickel is to be e-beam evaporated to about 1 μm thickness. If the source is Terfenol-D, it is also compatible is this process flow, as it can be sputtered in this step. In our initial actual fabrication trials for the deposition, we tried thermal evaporated copper as a seed layer and electroplated nickel in-house instead of the e-beam PVD process. The resulting layer showed good magnetic quality. Finally, the robots are extracted after release by Remover PG and cleaning. The finished μMAB's exhibit a slightly out-of-plane arched shape due to in-plane residual stresses.

IV. EXPERIMENTAL TESTING

A. Test-bed Design

To participate in the NIST Mobile Microrobotics Challenge at the 2010 IEEE International Conference on Robotics and Automation (ICRA) held in Anchorage, Alaska, a portable microrobotics test-bed was required to be designed and built to enable repeatable live demonstrations. Therefore, the system components were designed for easy assembly and disassembly and to fit the competition size constraints as

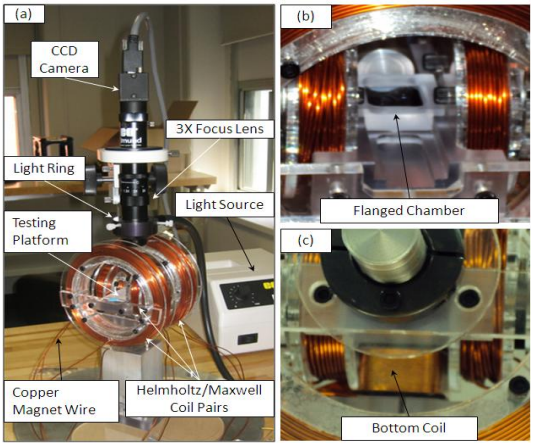

Fig. 3. Portable microrobotics test-bed

shown in Fig.3(a). It includes two orthogonal coil pairs that surround a testing platform where the robot moves, which are supported by a machined aluminum column. Computer-controlled drive electronics modulate the coils' operating current and voltage signals.

The robots are actuated and controlled with the magnetic field generated by the coil pairs. The coils are made from copper magnetic wire with 110 and 180 turns, with diameters of 2.2" and 3.1", respectively. Solid iron cores can be inserted into each coil to strengthen the magnetic field. The coil pairs are supported by laser-cut acrylic braces along with the testing platform, creating a coil assembly unit. The coil assembly unit sits on two press-fit guide shafts and a threaded rod. A thumb-screw on the threaded rod allows for vertical adjustment of the coil assembly unit relative to the fixed support column. Subsequent to the competition, a bottom coil has been embedded under the working platform, made of 50 turns of copper tape (Fig.3(c)). With constant current flow through the bottom coil, it can pull down the robot piece to the working plane so we can more easily obtain and observe the oscillating working mode of the robot due to in-plane field and strain. Because of the narrow working space, a simple flanged chamber (Fig.3(b)), made from acrylic, has also been added that can easily slide in and out. We can fill the chamber with water or any type of substrate to act as the working plane of the robot. The robot's performance is observed through an overhead firewire CCD camera (Flea2, Point Grey Research, Inc., *www.ptgrey.com*), a 0.7X to 3X focus lens (VZM 300i, Edmund Optics, *www.edmundoptics.com*), fiber optic light source and light ring (MI-150, Edmund Optics). The camera and lens are mounted on a rack and pinion focusing mount (NT54-793, Edmund Optics) that is attached to a vertical shaft on a circular baseplate. The camera is connected to a control computer to capture real-time images of the robot.

The drive electronics box is hooked up to two 35V/10A variable power supplies, each with two channels. Since the magnetic field is determined by the amount of current flowing through the coils, the drive electronics were designed to adjust the level of current through each coil independently. A series of solid state relays are used to control which of the four coils are activated. Power resistors and supply voltages are set to determine appropriate coil current levels. Two sets of power resistors (5 and 10 Ohm resistances) are used, allowing for high and low power mode operations for each of the coils. The modes are selected with a switch on the drive electronics control box. Also through a switch on the box, the two orthogonal coil pairs can be set to operate in either Helmholz or Maxwell coil pair configurations, allowing for the same or opposite current directions through the coils in the pair, respectively. Four relays are used to control one small coil and one big coil (i.e. one of the two coils in the coil pair). The relays (coils) can be opened and closed individually or simultaneously. The electronics have been designed to provide either constant or pulsed signal waveforms to the coils yielding constant or oscillating external fields to the robot workspace. These control signals, along with the control signals to operate the solid state relays, are sent via computer control of a data acquisition board (LabJack U3-HV and CB15 Board, *www.labjack.com*). The system is able to pulse signals with a frequencies as high as 100 kHz, which will cover the range of the first few natural frequencies of the μMABs. The electronics can provide up to 6 A of current per coil. With an input current of 2 A in one coil pair, a magnetic field of about 0.5 mT is able to be produced at the center area of the coil pairs, which is enough to drive the robot on a dry, flat substrate. A Matlab©-based graphical user interface was created to operate the system.

B. Testing and Results

Rectangular testing arena borders were constructed by patterning SU-8 photoresist. These hollow rectangular structures have inside dimensions of *3500* μm $\times$ textit2000 μm with line widths of *50* μm-*100* μm and a height of approximately *50* μm. They were released from the substrate after photoresist development so that they can be placed on top of various substrates for microrobot testing. Microrobot testing was performed on substrates of glass, silicon wafers (both polished and unpolished surfaces), and a combination of sputtered zirconia with a very thin ($\approx$250Å) over-layer of sputtered silica. Testing was conducted with the substrates open to atmospheric conditions as well as some tests with a plastic enclosure surrounding the test-bed and a low flow of nitrogen gas from above to help produce a clean, dry environment for the robots. A number of robots were selected from a couple of fabrication cycles for testing. Most of them are able to move in the magnetic field generated by one single coil. However, the initial tests utilizing glass substrates in an open testing environment provided inconsistent results. The same set of control signals resulted in varied robot performance, ranging from no movement to the robot being driven right off the test-bed at very high speeds. It was determined that the friction forces encountered between the robots legs and the glass substrate were too large and inconsistent to allow for controlled movements. Subsequent tests utilizing the silicon wafer substrates (both polished and unpolished surfaces) and the zirconia/silica substrates, with and without nitrogen, provided more consistent and repeatable results.

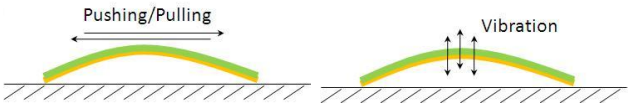

(a) Pushing/Pulling with Gradient Fields (b) Vibration Actuation from Oscillating Field

Fig. 4. μMAB actuation modes

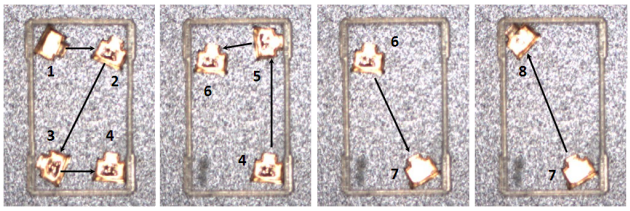

Fig. 5. Gradient field actuation: μMAB XY and diagonal translation

The expected actuation modes for the μMABs are shown schematically in Fig.4 and both were observed during the experiments. The first operating mode is pushing/pulling the magnetic body with a magnetic field (Fig.4(a)). In this mode, the magnetized nature of the robot is responsible for the motion. Different currents are input into each coil in a coil pair (small or large) to create a gradient magnetic field to direct the magnetic force and this results in translation of the μMAB on a dry surface with very fast speeds. This mode was used very successfully in the Two Millimeter Dash event at the challenge. The μMAB achieved one of the fastest individual runs of the competition for the dash at only 27 ms. Moreover, the translation direction for the μMAB is along the magnetic field line, which means the translation direction is predictable and controllable. Thus, by creating gradient fields with adjacent coils in the orthogonal sets in different pairs (i.e. one small coil and one large coil) diagonal translation is possible. We took advantage of this controllability in the Freestyle event in the competition, realizing automated horizontal, vertical and diagonal translation through a simple series of commands. Screen-shots illustrating the μMAB's performance under this gradient field actuation are shown in Fig.5.

Since the competition, we tested the robot's performance with the new testbed components and in a fluid environment for more uniform, larger damping and better control. The bottom coil was also utilized to increase the stability of the μMAB's movement. Much smoother movement trajectories were realized in the chamber filled with water. A curvilinear C-shaped path on the substrate was successfully traversed. Similar continuous translation tests were conducted, which were composed to trace out our school's initials, S-I-T, with the robot. The trajectories from these experiments were extracted off-line using the image processing toolbox in Matlab© and are shown in Fig.6 and Fig.7.

The second actuation mode is due to induced vibration of the robot from an oscillating (pulsing) magnetic field based on the magnetostrictive mechanism. A pulsed frequency of approximately 6 kHz was applied to the small coil pair, in the Helmholz configuration and the high power mode ($\approx$ 3A/coil), in 20 pulse increments. The pulse signal caused

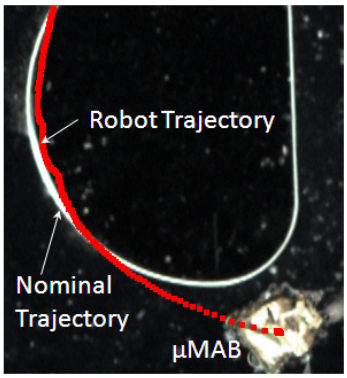

Fig. 6. μMAB trajectory for controlled translation in curvilinear locus

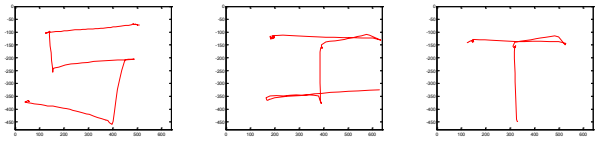

Fig. 7. μMAB trajectories for controlled translation in "SIT" locus

the main body of the robot to vibrate/deflect and the robot to translate across the substrate. At the conclusion of the pulse train, the robot motion ceased. Upon the application of another magnetic field pulse train, robot movement resumed in a similar manner. Snap-shots from one such test illustrating this actuation mode are shown in Fig.8. In this working mode, the robot moves relatively steady and controllable because the end point of each "walking" step is predictable and in limited distance. The bottom coil is on with constant current at the same time, pulling the robot body down for steady gait. Although the translation direction is not accordant with the robot's front and rear leg as expected, it shows different light reflections between stable and moving phase, which indicates the film vibrating. It also shows that the deflection power (force) is much bigger than the frictional resistance generated by gravity, because even a friction difference, not due to the asymmetric structure, is able to translate the robot.

V. DISCUSSION AND FUTURE WORK

The obtained μMAB performance revealed some important points for future improvements. The main problem is having the μMAB's exhibit the necessary deflections to allow the vibration mode actuation of the robot to occur.

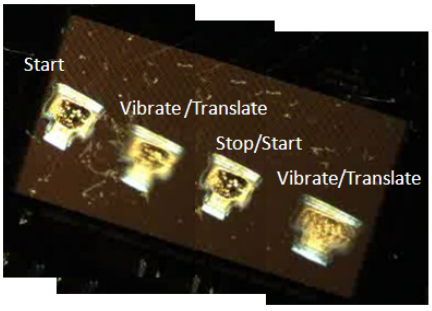

Fig. 8. Pulsed field actuation: μMAB vibration and translation

Only a small ratio out of all the robots tested were able to move in the vibration mode as designed, while all robots with a sufficient nickel layer translated in response to the application of gradient magnetic fields. Three main reasons for this type of performance and resulting recommendations for future work will be explained now.

In the magnetic domain, all the material with magnetic properties is initially magnetized. Therefore, it is extremely hard to determine how the magnetized body and magnetostrictive principle of the body are coupled and interact at the micro-scale. Therefore, more accurate theoretical modeling of the planar magnetostrictive bimorph, considering the initial magnetization is necessary for a better prediction of the robot's real performance.

Based on the design principle, the robot body's thickness is critical for the deflection while it is difficult to control this vertical dimension's accuracy using the current fabrication process. Due to this thickness uncertainty, the actual natural frequency of the robot can vary a lot from the analysis, which makes the determination of the input pulsing signal's frequency much more difficult. Improved or new strategies in the manufacturing process are called for in order to obtain more accurate geometric dimensions.

The surface condition (roughness, scratches) is a also key factor of the robot's performance. Flat and consistent non-smooth surfaces are the best for this robot design. For the pulling/pushing mode, the dry surface can lead to fast dashing while smooth and stable translation can be realized in fluid. The second oscillating operation mode needs a solid surface and a downward pulling force generated by the bottom coil helps with this mode. Thus, future work on fabricating a closed system with a sealed space for the robot's arena, conveniently designed for placing in and taking out the robots, will be pursued.

VI. CONCLUSIONS

A new wireless microrobot design, utilizing an asymmetric magnetostrictive bimorph structure was presented here. The magnetic field was generated by two pairs of magnetic coils which are controlled with a high current drive electronics package and a PC. The obtained results reveal that the magnetic and magnetostrictive principles are promising to actuate the microrobots with two wireless operating modes. A low magnetic field intensity and gradient have enough energy to power the microrobot. A more complicated microrobot design should be feasible by suitable application of structures using magnetostrictive mechanisms. The results also indicated that more realistic theoretical and FEM calculations are essential to capture the coupling effect of the magnetization and magnetostrictive phenomenon and accurately predict the microrobot performance. Finally, the working environment for the microrobot greatly affect its performance.

VII. ACKNOWLEDGMENTS

The authors would like to acknowledge Prof. Jan Nazalewicz, Mr. Yosef Korogodsky, and Mr. Rino DeFlorio for their help and discussions on the drive electronics. We also acknowledge the Micro-Devices Laboratory at Stevens Institute of Technology, Prof. E.H. Yang, Dr. Daizong Li, and Mr. Anderson Tsai, for providing the fabrication facility and required equipment training needed for this project. The authors would also like to acknowledge Dr. Craig McCray and Dr. Jason Gorman at NIST for organizing the NIST Mobile Microrobotics Challenge, for their discussions on the competition and all of the participants at the competition for their instructive comments.

REFERENCES

[1] J. J. Gorman, C. D. McGray, and R. A. Allen, "Mobile microrobot characterization through performance-based competitions," Performance Metrics for Intelligent Systems (PerMIS) Workshop, 2009.

[2] S. Hollar, A. Flynn, C. Bellew, and K. S. J. Pister, "Solar powered 10 mg silicon microrobot," in Proc. 16th Annu. Int. Conf. MEMS, 2003, pp. 706–711.

[3] B. R. Donald, C. Levey, C. D. McGray, I. Paprotny, and D. Rus, "An untethered, electrostatic, globally controllable mems microrobot," Journal of Microelectromechanical Systems, vol. 15, no. 1, pp. 1–15, 2006.

[4] O. J. Sul, M. R. Falvo, R. M. I. Taylor, S. Washburn, and R. Superfine, "Thermally actuated untethered impact-driven locomotive microdevices," Applied Physics Letters, vol. 89, no. 203512, 2006.

[5] E. Y. Erdem, Y.-M. Chen, J. W. Suh, G. T. A. Kovacs, and K. F. Bohringer, "Thermally actuated omnidirectional walking microrobot," Journal of Microelectromechanical Systems, vol. 19, no. 3, pp. 433–442, 2010.

[6] M. R. Pac and D. O. Popa, "Laser-powered sub-mm untethered microrobitcs," in Proc. Int. Conf. ASME IDETC, Montreal, Canada, Aug. 2010.

[7] K. Oldham, R. Choong-Ho, R. Jeong-Hoon, R. Polcawich, and J. Pulskamp, "Lateral thin-film piezoelectric actuators for bio-inspired micro-robotic locomotion," in Proc. Int. Conf. ASME IDETC, San Diego, CA, 2009.

[8] K. Vollmers, D. R. Frutiger, B. E. Kratochvil, and B. J. Nelson, "Wireless resonant magnetic microactuator for untethered mobile microrobots," Applied Physics Letters, vol. 92, no. 144103, 2008.

[9] C. Pawashe, S. Floyd, and M. Sitti, "Modeling and experimental characerization of an untethered magnetic micro-robot," Int. J. Robotics Research, 2009.

[10] S. Floyd, C. Pawashe, and M. Sitti, "An untethered magnetically actuated micro-robot capable of motion on arbitrary surfaces," in Proc. Int. Conf. IEEE on Robotics and Automation, Pasadena, CA, 2008.

[11] Nist mobile microrobotics challenge. National Institute of Standards and Technology. Gaithersburg, MD. [Online]. Available: http://www.nist.gov/eeel/semiconductor/mmc/

[12] J. Kim, J. Park, S. Yang, and et. al., "Establishment of a fabrication method for a long-term actuated hybrid cell robot," Lab on a chip, no. 7, pp. 1504–1508, 2007.

[13] P. Marcus, "Magnetostrictive bending of a cantilevered film-substrate system." Magnetism and Magnetic Materials, vol. 168, pp. 18–24, 1997.

[14] C. Sasso, M. Pasquale, L. Giudici, and et. al., "Piezomagnetic coefficients of polymer bonded co-ferrites," Sensors and Actuators A, vol. 129, pp. 159–162, 2006.

[15] IEEE Std 1976-1978 IEEE Standard on Piezoelectricity, IEEE Std., 1978.

[16] B. Jaffe, R. Cook, and H. Jaffe, Piezoelectric Ceramics. New York, NY: Academic Press, 1971.

[17] F. C. Fabrice, S. A. Wilson, G. Ensell, and et. al., "Characterization of pzt thin film micro-actuators using a silicon micro-force sensor," Sensors and Actuators A, vol. 133, pp. 35–44, 2007.

[18] Terfenol-d datasheet. Etrema Products, Inc. Ames, IA. [Online]. Available: http://www.etrema-usa.com/documents/Terfenol.pdf

[19] H. Janocha, "Application potential of magnetic field driven new actuators," Sensors and Actuators A, vol. 91, pp. 126–132, 2001.

[20] G. E. Owen, Electromagnetic Theory. Chelmsford, MA: Courier-Dover Publications, 2003.